Dynamic Rolled Sheets

Deutsche Ausgabe: DOI: 10.1002/ange.201607143
Internationale Ausgabe: DOI: 10.1002/anie.201607143

Static and Dynamic Nanosheets from Selective Assembly of Geometric Macrocycle Isomers

*Yanqiu Wang, Yongju Kim, and Myongsoo Lee**

Abstract: *In contrast to the significant advances that have been made in the construction of two-dimensional (2D) nanostructures, the rational modification from static to dynamic 2D sheets remains a great challenge. Static and dynamic sheets formed from selective self-assembly of geometric macrocycle isomers based on anthracene units are presented. The self-assembly of the cis isomer generates static planar sheets, whereas the trans isomer forms dynamic rolled sheets which are reversibly unrolled upon stimulation by a thermal signal. Furthermore, the mixed solution of the two isomers exhibits self-sorting behavior, generating the coexistence of the two independent self-assembled structures, the planar sheets and the folded scrolls. The self-sorted supramolecular objects with considerable shape and size differences are able to be readily separated, one isomer from the other.*

The construction of two-dimensional (2D) nanostructures is a fascinating target owing to their promising applications in areas ranging from nanotechnology to biotechnology, but they are challenging to synthesize without using 2D templates.[1] Such flat nanostructures with extremely high aspect ratios can be prepared by solution self-assembly of flat 2D aromatic building blocks such as disc-shaped molecules and aromatic macrocycles,[2] along with numerous metal–organic frameworks.[3] When the geometry of rigid aromatic cores is C_3-symmetric, the flat aromatic components self-assemble through side-by-side hydrogen bonding interactions[4] or host–guest complexations[5] to form stable, single layered nanostructures. The lateral association of nanofibers is an alternative strategy to construct flat 2D nanostructures. For example, the hydrophilic nanofibers with hydrophobic side faces laterally associate through side-by-side hydrophobic interactions to form planar structures.[6]

Along with the static 2D structures, flat structures are able to roll-up to form curved structures such as scrolls when they have a different up and down surface.[7] For example, polymer bilayers consisting of two different polymeric sheets exhibiting different swelling behavior can undergo folding upon solvation or temperature changes.[8] Surface-grafted nanosheets with grafting anisotropy provide another example for rolling-up into tubular scrolls because of the differences in the graft densities between the two surfaces of the sheets.[9] Besides multicomponent systems, the self-assembly strategy is a useful means for the construction of homogeneous nanostructures exhibiting self-rolling behavior.[10] When aromatic segments based on an imidazole unit self-assemble into a single layer, for example, the hydrogen bonding asymmetry between up and down planar surfaces drives the planar structure to roll up into scrolls owing to different surface tension.[11] Along with surface anisotropy, self-folding can be achieved by packing changes in aromatic crystals. For example, the aromatic macrocycle dimers based on anthracene units self-assemble into highly curved structures driven by molecular sliding of anthracene stacks.[12] However, all of these self-assembly approaches based on crystal packings, grafting anisotropy, and hydrogen bonding asymmetry could not offer a direct means to allow dynamic structural changes without breaking. To create robust self-assembled sheets with dynamic shape changes, it is necessary to design sophisticated aromatic assembly that is sensitive to small local changes in the interactions between the molecular modules and the external energy supply.

Herein, we report static and dynamic nanosheets formed from selective self-assembly of geometric macrocycle isomers based on anthracene units (Figure 1). Both *cis* and *trans* isomers self-assemble into 2D sheet structures through lateral association of primary nanofibers in aqueous solution. However, the self-assembly of the *cis* isomer generates static planar sheets, while the *trans* isomer forms dynamic rolled sheets that are reversibly unrolled in response to a thermal signal. Furthermore, the mixture solution of the two isomers exhibits self-sorting behavior, generating the coexistence of

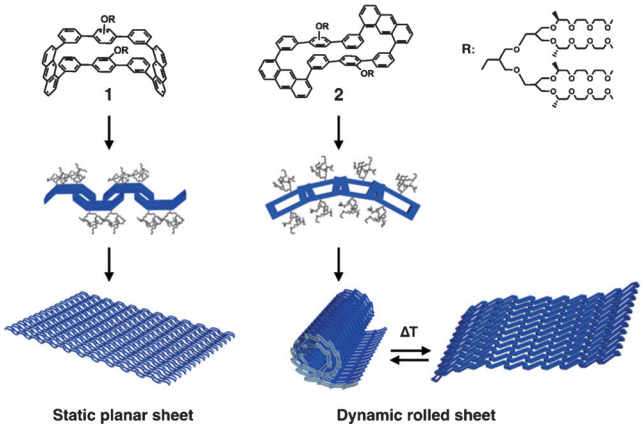

Figure 1. Molecular structures of *cis* and *trans* macrocycle isomers and a representation of static planar sheets and dynamic rolled sheets.

[*] Y. Wang, Dr. Y. Kim, Prof. M. Lee
State Key Laboratory of Supramolecular Structure and Materials, College of Chemistry, Jilin University
Changchun 130012 (China)
E-mail: mslee@jlu.edu.cn

Supporting information for this article can be found under: http://dx.doi.org/10.1002/anie.201607143.

the planar sheets and the scrolls. The self-sorted supramolecular structures with considerable differences in size and shape are able to separate readily from one another using gel permeation chromatography (GPC), which allows facile separation of the *cis* and *trans* macrocycle isomers into their pure components.

Amphiphilic macrocycle isomers were synthesized in a stepwise fashion according to the procedures described in the Supporting Information. The *cis* and *trans* isomers were synthesized and characterized by NMR spectroscopy and MALDI-TOF mass spectroscopy (Supporting Information, Figures S1–S4), and the results were in full agreement with the structures presented herein. The formation of self-assembled nanostructures was initially investigated by transmission electron microscopy (TEM) and fluorescence optical microscopy (FOM). The images of the *cis* isomer, **1** showed 2D sheet structures with the in-plane parallel arrangements of the primary nanofibers (Figure 2a), demonstrating that the

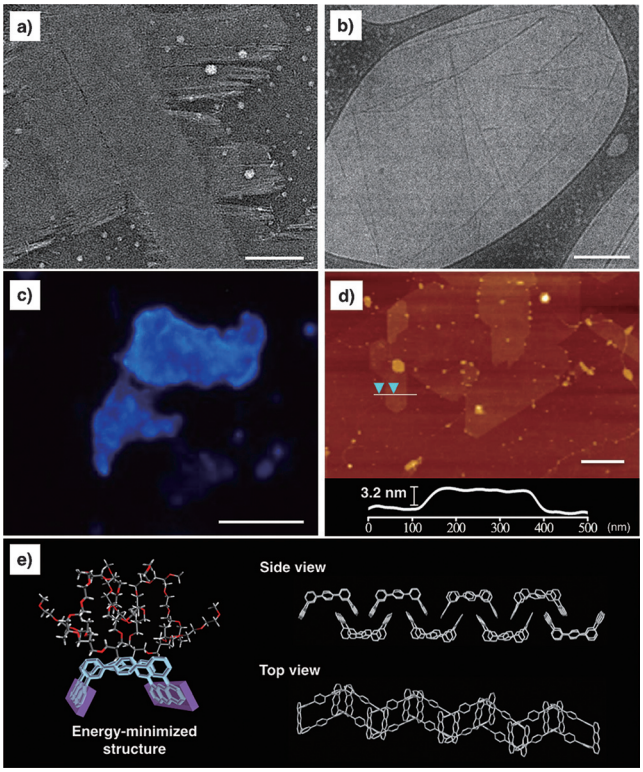

Figure 2. a) Negative-stain TEM image of **1** from 0.01 wt% aqueous solution. Scale bar: 100 nm. b) Cryo-TEM image of **1** from 0.01 wt% aqueous solution. Scale bar: 200 nm. c) FOM image of **1** from 0.01 wt% aqueous solution (excitation filter at λ_{ex} = 340–480 nm). Scale bar: 5 μm. d) AFM height image of **1** from 0.01 wt% aqueous solution. Scale bar: 100 nm. e) Molecular dynamic simulations result of **1** in a water environment. Dendrimers are omitted for clarity.

preformed nanofibers laterally associate to generate planar sheet structures. The formation of the flat nanostructures was also confirmed using cryogenic TEM (Cryo-TEM), which showed sheet-like objects with straight edges (Figure 2b), indicating that the sheets are robust and free-standing in bulk solution. The edge lengths are typically from several hundreds of nanometers to few micrometers. Additional structural information of the sheets was obtained by FOM (Figure 2c) and atomic force microscopy (AFM) measurements on a hydrophilic mica substrate in the completely dried state (Figure 2d). The AFM image of **1** revealed planar sheets with a thickness of 3.2 nm, which is consistent with the expected thickness of single layers.

Circular dichroism (CD) spectroscopy measurements revealed apparent CD signals in the spectral range of the aromatic segment, indicating that the in-plane nanofibers of the 2D sheets are based on a helical structure with a chiral bias (Supporting Information, Figure S5).[13] To understand the chiral primary structure of the 2D assembly, molecular dynamic simulations were performed using Desmond from Schrödinger Suites (Figure 2e). The simulations of **1** showed that the aromatic macrocycle adopts a concave configuration with the upward positioning of the two oligoether dendrons where the anthracene units at both ends of the concave macrocycle are twisted with respected to each other, generating intrinsic molecular chirality.[14] The concave macrocycles are alternatively up and down within the row in an undulated arrangement (Figure 2e, side view), in which the adjacent anthracene stacks are twisted in a zig-zag fashion (Figure 2e, top view) so as to decrease the surface stress. According to the simulations, the aromatic side faces of the primary fibers are not entirely surrounded by hydrophilic chains. To reduce the contact between aromatic segments and water molecules, the helical fibers laterally assemble into 2D planar structures (Figure 1).[15] Notably, the planar structures maintain even at higher temperatures without any noticeable structural changes, indicating that the 2D structures are static within the temperature range of our investigations. This is consistent with a lack of any noticeable spectral changes in UV absorptions, fluorescence emissions, and CD spectra, irrespective of temperature changes (Supporting Information, Figure S6).

In great contrast to the robust planar sheet structures of **1**, the 2D sheets of the *trans* isomer, **2** spontaneously roll up into highly-curved scrolls, which undergo reversible unrolling triggered by an external signal (Figure 1). As shown in Figure 3, TEM revealed that the *trans* isomer self-assembles into flexible nanofibers at the initial stages of self-assembly (10 min), which are arranged parallel to each other to form flat sheets after 30 min (Figure 3a,b). Subsequently, the sheets spontaneously roll-up perpendicular to the fiber long axis into closely-packed scrolls with an external diameter of about 40 nm (Figure 3c). Cryo-TEM revealed that the internal diameter of the tubular scroll is about 25 nm, indicating that the scrolls consist of multilayer walls (Figure 3d). CD spectroscopy measurements revealed that the signals appear after 30 min aging at ambient conditions, which become more apparent with increasing aging time up to 3 h (Figure 3e). These results, together with the time-dependent TEM data, suggests that the adjacent aromatic macrocycles are twisted with respect to each other in one direction, which drives the planar sheets to fold perpendicular to the fiber axis into closely packed scrolls. Indeed, the absorption maximum associated with the anthracene unit at about 400 nm was red-shifted by 11 nm over that of the molecularly dissolved state,

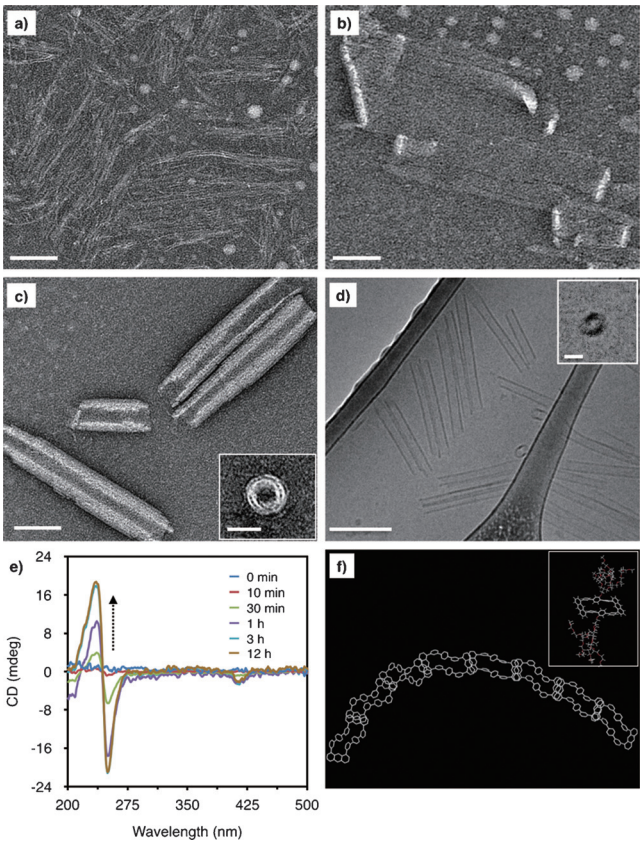

Figure 3. Time-dependent TEM images of **2** from 0.01 wt% aqueous solution after aging a) 10 min, b) 30 min and c) 3 h. Scale bars: 50 nm. Inset image is a top view of the tubular scroll. Inset scale bar: 30 nm. d) Cryo-TEM image of **2** from 0.01 wt% aqueous solution. Scale bar: 100 nm; inset is top view cryo-TEM image; scale bar: 20 nm. e) Time-dependent CD spectra of **2** from 0.01 wt% aqueous solution. f) Molecular dynamics simulation of **2** in the water environment. Dendrimers are omitted for clarity.

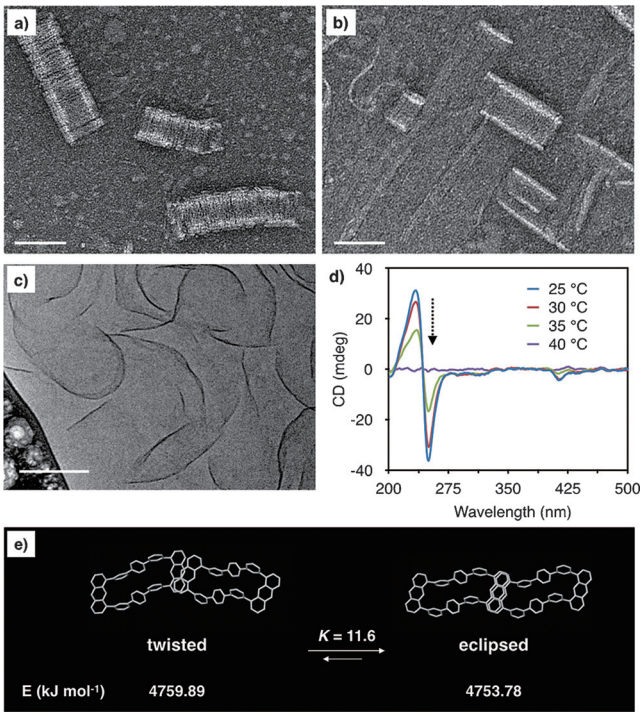

Figure 4. a), b) Negative-stain TEM images of **2** from 0.01 wt% aqueous solution at a) 35 °C and b) 38 °C. Scale bars: 50 nm. c) Cryo-TEM image of **2** from 0.01 wt% aqueous solution at 42 °C. Scale bar: 100 nm. d) Temperature-dependent CD spectra of **2** from 0.01 wt% aqueous solution. e) Molecular dynamics simulations with a dimer of **2** in hydrophobic octanol environment. Dendrimers are omitted for clarity.

indicating that the anthracene stacks in the scrolls are twisted relative to each other (Supporting Information, Figure S7).[16]

To gain further insight into the origin of the curvature of the self-assembled layer, we performed dynamics simulations (Figure 3 f). Using the *trans* conformation of the macrocycle, we optimized the structure until eight molecules are arranged in a stabilized fiber. The simulations showed that the single fiber is spontaneously curved with the folding axis perpendicular to the fiber axis direction. As the macrocycles are arranged in a row through the anthracene stacking interactions, the two adjacent anthracene units are somewhat slipped and twisted with respect to its neighbor to reduce steric hindrance between the adjacent hydrophilic dendritic segments.[17] Along with the spectroscopic data, our simulations further support that the rolling of the sheets originates from the slipped and twisted stacking of the two adjacent anthracene units. Consequently, this twisted packing of the anthracene units which are packed perpendicular to the layer plane gives rise to rolling the sheets with the axis perpendicular to the fiber direction (Figure 1).

Interestingly, the scrolls undergo reversible unfolding at 40 °C at which the oligoether chains undergo dehydration.[15,18] Upon heating to 37 °C, the closely-packed scrolls are gradually loosened (Figure 4 a) and subsequently transform into open sheets (Figure 4 b). Cryo-TEM taken at 42 °C revealed flexible sheets, indicating that the scrolls unfold into flat sheets upon stimulation by a thermal trigger (Figure 4 c). Complete recovery to the original scrolls was observed over 12 h of resting at room temperature (Supporting Information, Figure S8a), indicating that the scrolls undergo reversible switching between folding and unfolding states. This was further confirmed by CD measurements as a function of temperature (Figure 4 d). On heating, the CD signal gradually decreased up to 35 °C and then disappeared at 40 °C. When cooled to 25 °C, we observed complete recovery of the original CD profile, which is consistent with the observations from TEM (Supporting Information, Figure S8b).

The reversible folding and unfolding switch of the scrolls is attributed to the thermal dehydration of the dendritic ethylene oxide chains in aqueous media.[18,19] At room temperature, the macrocycles are twisted with respect to their neighbors to reduce steric repulsions between adjacent hydrated dendritic segments with an open-chain conformation. On heating, however, the shrunken oligoether chains caused by dehydration would make the twisted stacking of the macrocycles to be unstable owing to enthalpic penalty associated with twisted anthracesne packings in hydrophobic environments. To relieve the enthalpic penalty, the anthracene planes would be eclipsed to maximize aromatic inter-

actions between them, thus lowering total free energy. Indeed, the calculations showed that the non-curved structures originated from the eclipsed packings of the anthracene units are more favorable than the curved structures based on the twisted packings in a hydrophobic environment, as opposed to that in the water environment (Figure 4e). This is further supported by blue-shifted absorption maximum associated with the anthracene unit (Supporting Information, Figure S9a), fluorescence quenching (Figure S9b), and disappearance of the CD signals upon heating.

One of the fascinating features in biological systems is that different molecular components, such as proteins, carbohydrate polymers, and lipid molecules, independently self-assemble into distinct supramolecular aggregates without affecting each other.[20,21] These self-assembly processes originate from the self-sorting of their molecular components, which allow the coexistence of different functional architectures which act independently within a single system.[22,23] Inspired by these biological processes, we envisioned that the mixture of the *cis* and *trans* isomers would exhibit self-sorting behavior owing to their distinct molecular shapes.[24] With this idea in mind, we prepared a solution of a 1:1 mixture of **1** (*cis* isomer) and **2** (*trans* isomer) in THF, added water in this solution and slowly removed the organic solvent at ambient conditions. Cryo-TEM investigations of the mixture solution revealed the coexistence of scrolls and flat sheets (Supporting Information, Figure S10), suggesting that the *cis* and *trans* macrocycles self-recognize by themselves to form two distinct self-sorted structures, that is, unfolded sheets and folded scrolls. Close examinations of the image revealed that the size of the sheets in edge dimensions is ranging from several hundreds of nanometers to few micrometers, whereas the folded scrolls appear to be smaller in both length and diameter than the edge dimensions of the sheets. Considering the considerable shape and size differences between the sheets and the scrolls, we considered that the two self-sorted supramolecular objects can be readily separated by gel permeation chromatography (GPC), as the larger flat structures are eluted first over the smaller folded scrolls. Indeed, a GPC chromatogram using a Sephacryl S-500HR column showed multiple peaks including an isolated first-eluted fraction (I), next-eluted mixed fractions (II), and then another isolated last-eluted fraction (III; Figure 5a). As expected, TEM revealed that the first fraction consists of the large sheets and the last fraction consists of the folded scrolls (Supporting Information, Figure S11). The fraction II showed the coexistence of open sheets and closed tubular, which correspond to the mixture of *cis* and *trans* isomers (Figure 5b).

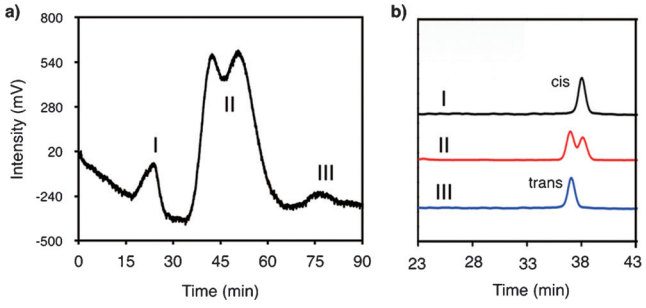

Figure 5. a) GPC chromatogram of the mixture solution. b) HPLC chromatograms of each fraction from GPC.

To identify the pure macrocycle isomers, each of the fractions was subjected to analytical high-performance liquid chromatography (HPLC; Figure 5b). The HPLC chromatograms of the first fraction (I) associated with the sheet-like objects and the last fraction (III) associated with the scrolls showed respective single peaks, corresponding to the *cis* and *trans* isomers, respectively. These results demonstrate that the two isomers independently self-assemble into distinct supramolecular aggregates in a single system without influencing each other. Beyond the self-assembly, our results indicate that the geometrical isomers with delicate differences in their molecular structure can be readily separated from one another through the self-sorting processes. The self-sorting of the geometric macrocycle isomers is considered to originate not only from the different geometries of the two isomers but also from the different spatial orientations of the flexible chains of the isomers. The energy-minimized structure of the *cis* isomer showed that both dendritic chains are located at the concave face of the macrocycle plane (Figure 2e), while the two dendrimers in the *trans* isomer are positioned opposite each other on the sides of the macrocycle plane (Figure 3f), approximately similar to other isomers based on anthracene.[25] These configurational and conformational differences of the two isomers lead to self-recognition through orthogonally operating noncovalent interactions to form self-sorted structures.[26] Another important point to be noted is that such a geometry-selective recognition event provides a promising strategy for the facile separation of geometrical isomers with subtle differences in their molecular structures.

In conclusion, we have demonstrated that the geometrical isomers of macrocycles selectively self-assemble into distinct nanosheet structures in aqueous solutions. The macrocycle isomer based on a *cis* geometry forms static planar sheets, whereas the *trans* one self-assembles into dynamic rolled sheets that undergo reversible unrolling upon stimulation by a thermal trigger. The dynamic switching feature of the scrolls is attributed to reversible twisting of the two adjacent aromatic macrocycle stackings in a row arising from hydrophilic to hydrophobic environmental changes caused by thermal dehydration of the oligoether dendron side groups. Furthermore, the mixture solution of the two isomers exhibits self-sorting behavior, that is, the two isomers independently self-assemble into distinct supramolecular aggregates, planar sheets, and folded scrolls, in a single system without influencing each other. As the facile separation of the self-sorted supramolecular objects with the considerable shape and size differences, we are able to readily separate one isomer from the other. Our results will provide a new insight into not only the design of nanomaterials with static and dynamic switching, but also a novel approach for the facile separation of geometric isomers.

Acknowledgements

This work was supported by 1000 Program, NSFC (Grant 51473062, Grant 21574055, and Grant 21550110493).

Keywords: dynamic rolled sheets · geometric macrocycle isomers · selective assembly · self-sorting · static planar sheets

How to cite: *Angew. Chem. Int. Ed.* **2016**, *55*, 13122–13126
Angew. Chem. **2016**, *128*, 13316–13320

[1] a) J. Sakamoto, J. van Heijst, O. Lukin, A. D. Schlüter, *Angew. Chem. Int. Ed.* **2009**, *48*, 1030–1069; *Angew. Chem.* **2009**, *121*, 1048–1089; b) J. W. Colson, W. R. Dichtel, *Nat. Chem.* **2013**, *5*, 453–465.

[2] a) P. Kissel, R. Erni, W. B. Schweizer, M. D. Rossell, B. T. King, T. Bauer, S. Götzinger, A. D. Schlüter, J. Sakamoto, *Nat. Chem.* **2012**, *4*, 287–291; b) P. Kissel, J. van Heijst, R. Enning, A. Stemmer, A. D. Schlüter, J. Sakamoto, *Org. Lett.* **2010**, *12*, 2778–2781; c) Y. Kim, S. Shin, T. Kim, D. Lee, C. Seok, M. Lee, *Angew. Chem. Int. Ed.* **2013**, *52*, 6426–6429; *Angew. Chem.* **2013**, *125*, 6554–6557; d) Y. Kim, M. Lee, *Chem. Eur. J.* **2015**, *21*, 5736–5740.

[3] a) Y. Peng, Y. Li, Y. Ban, H. Jin, W. Jiao, X. Liu, W. Yang, *Science* **2014**, *346*, 1356–1359; b) L. Yue, S. Wang, D. Zhou, H. Zhang, B. Li, L. Wu, *Nat. Commun.* **2016**, *7*, 1074; c) R. Dong, M. Pfeffermann, H. Liang, Z. Zheng, X. Zhu, J. Zhang, X. Feng, *Angew. Chem. Int. Ed.* **2015**, *54*, 12058–12063; *Angew. Chem.* **2015**, *127*, 12226–12231.

[4] I. Hisaki, S. Nakagawa, N. Ikenaka, Y. Imamura, M. Katouda, M. Tashiro, H. Tsuchida, T. Ogoshi, H. Sato, N. Tohnai, et al., *J. Am. Chem. Soc.* **2016**, *138*, 6617–6628.

[5] K.-D. Zhang, J. Tian, D. Hanifi, Y. Zhang, A. C.-H. Sue, T.-Y. Zhou, L. Zhang, X. Zhao, Y. Liu, Z.-T. Li, *J. Am. Chem. Soc.* **2013**, *135*, 17913–17918.

[6] a) B. Shen, Y. He, Y. Kim, Y. Wang, M. Lee, *Angew. Chem. Int. Ed.* **2016**, *55*, 2382–2386; *Angew. Chem.* **2016**, *128*, 2428–2432; b) E. Lee, J.-K. Kim, M. Lee, *Angew. Chem. Int. Ed.* **2008**, *47*, 6375–6378; *Angew. Chem.* **2008**, *120*, 6475–6478.

[7] a) A. R. Studart, *Angew. Chem. Int. Ed.* **2015**, *54*, 3400–3416; *Angew. Chem.* **2015**, *127*, 3463–3479; b) R. Fernandes, D. H. Gracias, *Adv. Drug Delivery Rev.* **2012**, *64*, 1579–1589; c) J.-H. Kim, M. Bohra, V. Singh, C. Cassidy, M. Sowwan, *ACS Appl. Mater. Interfaces* **2014**, *6*, 13339–13343; d) E. Lee, J.-K. Kim, M. Lee, *Angew. Chem. Int. Ed.* **2009**, *48*, 3657–3660; *Angew. Chem.* **2009**, *121*, 3711–3714.

[8] a) O. G. Schmidt, K. Eberl, *Nature* **2001**, *410*, 168; b) T.-A. Asoh, M. Matsusakl, T. Kaneko, M. Akashi, *Adv. Mater.* **2008**, *20*, 2080–2083; c) L. Ionov, *Soft Mater.* **2011**, *7*, 6786–6791.

[9] M. Han, J. Hyun, E. Sim, *Soft Mater.* **2015**, *11*, 3714–3723.

[10] a) H.-J. Kim, T. Kim, M. Lee, *Acc. Chem. Res.* **2011**, *44*, 72–82; b) D.-J. Hong, E. Lee, M.-G. Choi, M. Lee, *Chem. Commun.* **2010**, *46*, 4896–4898.

[11] D.-J. Hong, E. Lee, H. Jeong, J.-K. Lee, W.-C. Zin, T. D. Nguyen, S. C. Glotzer, M. Lee, *Angew. Chem. Int. Ed.* **2009**, *48*, 1664–1668; *Angew. Chem.* **2009**, *121*, 1692–1696.

[12] C.-M. Chou, S. Nobusue, S. Saito, D. Inoue, D. Hashizume, S. Yamaguchi, *Chem. Sci.* **2015**, *6*, 2354–2359.

[13] J. Kumaki, S.-I. Sakurai, E. Yashima, *Chem. Soc. Rev.* **2009**, *38*, 737–746.

[14] M. M. Safont-Sempere, P. Osswald, K. Radacki, F. Würthner, *Chem. Eur. J.* **2010**, *16*, 7380–7384.

[15] Y. Kim, J. Kang, B. Shen, Y. Wang, Y. He, M. Lee, *Nat. Commun.* **2015**, *6*, 8650.

[16] F. Würthner, T. E. Kaiser, C. R. Saha-Möller, *Angew. Chem. Int. Ed.* **2011**, *50*, 3376–3410; *Angew. Chem.* **2011**, *123*, 3436–3473.

[17] J.-K. Kim, E. Lee, M.-C. Kim, E. Sim, M. Lee, *J. Am. Chem. Soc.* **2009**, *131*, 17768–17770.

[18] a) W. Li, Y. Kim, J. Li, M. Lee, *Soft Mater.* **2014**, *10*, 5231–5242; b) W. Li, Y. Kim, M. Lee, *Nanoscale* **2013**, *5*, 7711–7723; c) Z. Huang, H. Lee, E. Lee, S.-K. Kang, J.-M. Nam, M. Lee, *Nat. Commun.* **2011**, *2*, 459.

[19] J.-F. Lutz, K. Weichenhan, Ö. Akdemir, A. Hoth, *Macromolecules* **2007**, *40*, 2503–2508.

[20] G. Vereb, J. Szöllősi, J. Matkó, P. Nagy, T. Farkas, L. Vígh, L. Mátyus, T. A. Waldmann, S. Damjanovich, *Prog. Nat. Acad, Proc. Natl. Acad. Sci. USA* **2003**, *100*, 8053–8058.

[21] G. M. Whitesides, B. Grzybowshi, *Science* **2002**, *295*, 2418–2421.

[22] A. Heeres, C. van der Pol, M. Stuart, A. Friggeri, B. L. Feringa, J. van Esch, *J. Am. Chem. Soc.* **2003**, *125*, 14252–14253.

[23] A. Wu, L. Isaacs, *J. Am. Chem. Soc.* **2003**, *125*, 4831–4835.

[24] a) M. M. Safont-Sempere, G. Fernández, F. Würthner, *Chem. Rev.* **2011**, *111*, 5784–5814; b) J. Boekhoven, A. M. Brizard, M. C. A. Stuart, L. Florusse, G. Raffy, A. Del Guerzoc, J. H. Van Esch, *Chem. Sci.* **2016**, DOI: 10.1039/C6Sc01021K; c) K. Aratsu, D. D. Prabhu, H. Iwawaki, X. Lin, M. Yamauchi, T. Karatsu, S. Yagai, *Chem. Commun.* **2016**, DOI: 10.1039/C6CC03419E; d) C. Rest, M. J. Mayoral, G. Fernández, *Int. J. Mol. Sci.* **2013**, *14*, 1541–1546; e) D. Görl, X. Zhang, V. Stepanenko, F. Würthner, *Nat. Commun.* **2015**, *6*, 7009.

[25] A. Suzuki, K. Kondo, M. Akita, M. Yoshizawa, *Angew. Chem. Int. Ed.* **2013**, *52*, 8120–8123; *Angew. Chem.* **2013**, *125*, 8278–8281.

[26] I. S. Choi, N. Bowden, G. M. Whitesides, *J. Am. Chem. Soc.* **1999**, *121*, 1754–1755.

Received: July 23, 2016
Published online: September 16, 2016

